Check for updates

ADVANCED MATERIALS
www.advmat.de

Gbits/s-Level Encrypted Spectral Wireless Communication Enabled by High-Performance Flexible Organic Hyperspectrometer

Hao Qin, Hanzhe Shi, Tingting Guo, Chen Geng, Weicai Li, Jingbo Zhao, Jing Zhang, Yu Zhu, Ruiman Han, Wangqiao Chen, Tiejun Lv, Guanghui Li, and Yongsheng Chen**

The exponential growth of data in the information era has pushed conventional optical communication technology to its limitations, including inefficient spectral utilization, slow data rate, and inherent security vulnerabilities. Here, a transformative high-speed organic spectral wireless communication (SWC) technology enabled by a flexible, miniaturized, and high-performance organic hyperspectrometer is proposed that integrates ultrahigh-speed data transmission with hardware-level encryption. By synergistically combining organic photodetector arrays with tunable responsivities and spectral-tunable organic filters, the organic hyperspectrometer achieves a broad spectral detection range of 400 to 900 nm, resolution of 1.08 nm, accuracy of 0.60 nm, and response time of 684 ns. Unlike prior optical wireless communication systems, the organic hyperspectrometer-based SWC platform uniquely decodes high-speed encrypted data at the hardware level, which is a breakthrough in secure, high-speed, and high-capacity communication. Harnessing the full visible-to-near-infrared spectrum, the SWC system achieves a theoretical data rate of 9.1 Gbits s^{-1}, ranking as the highest-speed organic optical communication system. Furthermore, the intrinsic flexibility and bandgap-tunability of organic materials enable unparalleled portability, adaptability, and scalability of organic SWC, establishing a scalable framework for terahertz-scale data transmission. These advancements mark a pivotal leap toward secure, high-speed, and ultracompact optical networks for the future data- and AI-driven era.

1. Introduction

The exponential surge in data driven by artificial intelligence (AI), autonomous systems, and hyperconnected IoT networks has pushed conventional wireless communication systems based on radio frequency to their limits in terms of data rate and security.[1–5] This demands a novel wireless communication system with ultrahigh-speed data transmission paired with unbreakable security. Optical wireless communication (OWC), which harnesses the vast yet underutilized bandwidth of the visible to near-infrared spectrum (400–800 THz), has emerged as a transformative solution for 5G/6G networks.[6] Despite achieving significant advances in transmission rates in laboratories by detecting specific single- or multi-wavelengths using photodetectors, OWC still suffers from two fundamental bottlenecks: 1. Inefficient spectral utilization of every monochromatic light across the broad visible-to-infrared range and limited data rate; 2. Inherent security vulnerabilities in open optical environments.[7–9] Although the existing state-of-the-art optical

H. Qin, H. Shi, T. Guo, C. Geng, J. Zhang, Y. Zhu, G. Li, Y. Chen
The Centre of Nanoscale Science and Technology and Key Laboratory of Functional Polymer Materials
Institute of Polymer Chemistry
Renewable Energy Conversion and Storage Center (RECAST)
College of Chemistry
Nankai University
Tianjin 300071, China
E-mail: ghli1127@nankai.edu.cn; yschen99@nankai.edu.cn

Y. Chen
State Key Laboratory of Elemento-Organic Chemistry
Nankai University
Tianjin 300071, China

The ORCID identification number(s) for the author(s) of this article can be found under https://doi.org/10.1002/adma.202513003

DOI: 10.1002/adma.202513003

Y. Chen
Frontiers Science Center for New Organic Matter
College of Chemistry
Nankai University
Tianjin 300071, China

G. Li
Academy for Advanced Interdisciplinary Studies
Nankai University (AAIS)
Nankai University
Tianjin 300071, China

R. Han, W. Chen
Guangdong Provincial Key Laboratory of Optical Information Materials and Technology
South China Academy of Advanced Optoelectronics
South China Normal University
Guangzhou 510006, China

W. Li, J. Zhao, T. Lv
School of Information and Communication Engineering
Beijing University of Posts and Telecommunications
Beijing 100876, China

 © 2025 Wiley-VCH GmbH

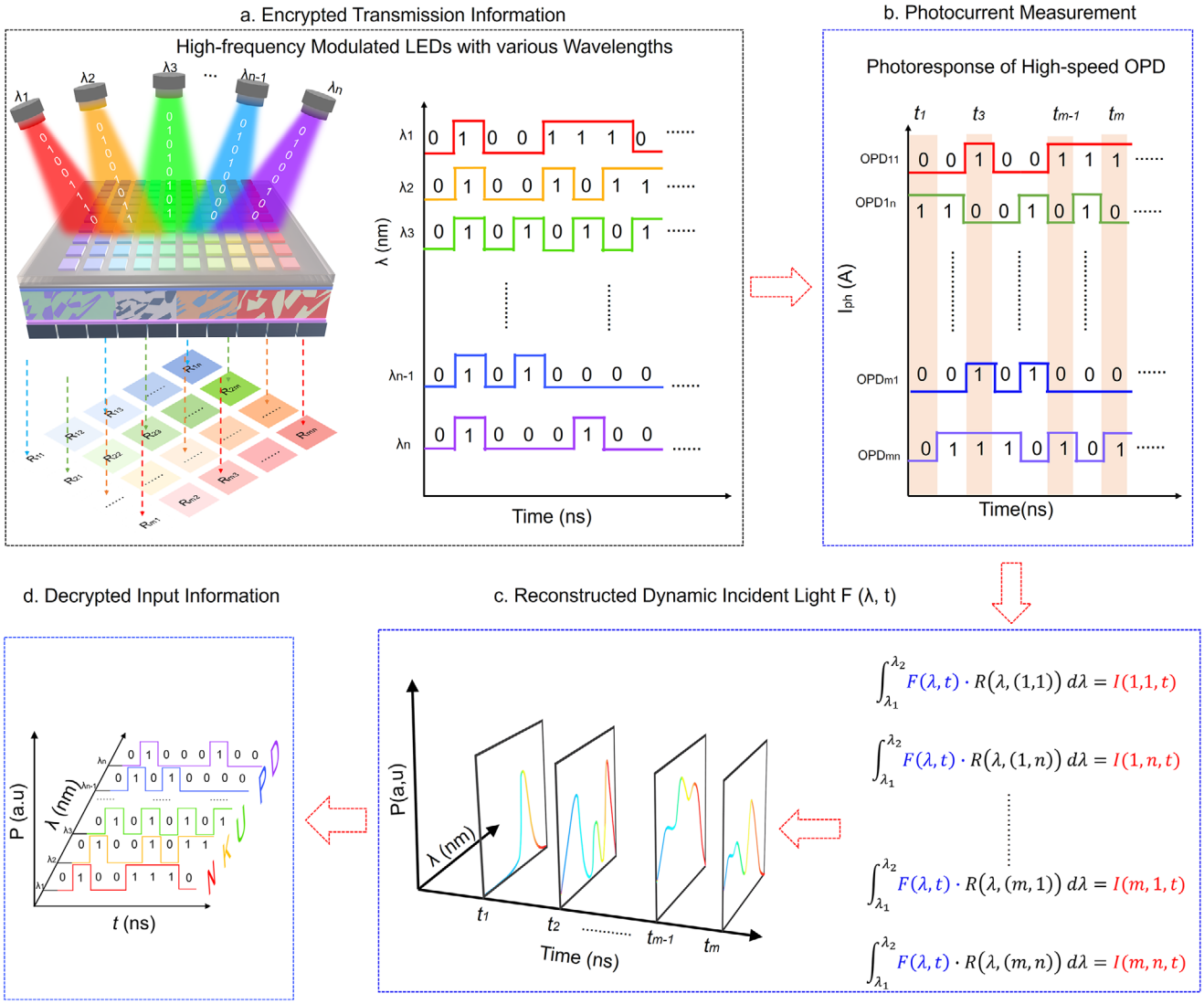

Figure 1. Spectral wireless communication concept based on a high-speed organic hyperspectrometer. a) Schematic of our organic hyperspectrometer based on an organic photodetector array with various responsivities irradiated by high-frequency modulated LEDs with various wavelengths. b–d) Schematic of SWC examples using an organic hyperspectrometer for high-speed encrypted information transmission: photodetector array to detect the photoresponse in the time domain, hyperspectrometer to resolve the spectra in the time domain, and decrypted the transmission data by analyzing the wavelength, frequency, and binary states of optical information.

multiple-input multiple-output (MIMO) architecture impressively improves transmission speed and capacity via parallel spatial channels, it remains constrained by finite spectral slices and demands precise beam alignment, thereby failing to exploit the whole spectrum fully.[10] Quantum key distribution offers unbeatable security through quantum mechanics, but struggles with impractically low data rates and limited operational ranges.[11,12] Meanwhile, traditional software-based encryption approaches are growing increasingly susceptible to AI-accelerated cryptanalysis and emerging quantum attacks.[13,14] Therefore, it is imperative to reconceptualize OWC architectures at the hardware level, which can seamlessly integrate ultrahigh-speed data transmission with physics-embedded encryption to achieve intrinsic spectral efficiency and security beyond conventional OWC.[15]

A particularly promising approach to this challenge is the high-speed spectral wireless communication (SWC) system, which can maximize spectrum efficiency to achieve an enhanced transmission rate.[16] Moreover, integrating the wavelength into the data transmission can significantly enhance information security by manipulating the wavelength, which encrypts input signals by concealing desired information within the wavelength.[17,18] To realize such an advanced system for modern electronics, the spectrometer, functioning as the core component of SWC, must have ultrafast response speed, broad bandwidth, high resolution, and high accuracy, alongside a miniaturized size, flexible, and lightweight architecture.[19,20] Despite conventional benchtop spectrometers exhibiting high spectral resolution and accuracy across broad spectra, they primarily depend on bulky optical components (e.g., gratings, interferometers, and filters)

© 2025 Wiley-VCH GmbH

15214095, 2026, 1, Downloaded from https://advanced.onlinelibrary.wiley.com/doi/10.1002/adma.202513003 by Yongsheng Chen - CAS-CHONGQING INSTITUTE OF GREEN & INTELLIGENT TECHNOLOGY , Wiley Online Library on [13/03/2026]. See the Terms and Conditions (https://onlinelibrary.wiley.com/terms-and-conditions) on Wiley Online Library for rules of use; OA articles are governed by the applicable Creative Commons License

15214095, 2026, 1, Downloaded from https://advanced.onlinelibrary.wiley.com/doi/10.1002/adma.202513003 by Yongsheng Chen - CAS-CHONGQING INSTITUTE OF GREEN & INTELLIGENT TECHNOLOGY , Wiley Online Library on [13/03/2026]. See the Terms and Conditions (https://onlinelibrary.wiley.com/terms-and-conditions) on Wiley Online Library for rules of use; OA articles are governed by the applicable Creative Commons License

that split the composite light into monochromic light beams by slowly moving these optical components, severely hindering their integration with lightweight electronics and slowing the spectrum acquisition speed.[19,21–23] In contrast, emerging miniaturized computational spectrometers based on either single-detector devices or photodetector arrays, merging wavelength multiplexing principles with advanced algorithms, have successfully scaled down the spectrometer to the submillimeter scale and realized significant improvement in critical metrics.[19] For example, the single-detector miniaturized spectrometers, such as those leveraging 2D materials,[24,25] perovskites,[26] and organic semiconductors,[27] primarily rely on sequentially and slowly modulating the responsivity of the photodetector by tuning gating/bias voltages,[25,28] strain applied on photoactive materials,[29] and spectral filters.[30] Alternatively, a photodetector array-based system that is fabricated with novel photoactive materials, such as nanowire arrays,[31] quantum dots,[32] and perovskites,[33,34] can realize simultaneous photocurrent collection for generating a photoresponse matrix generation and resolving spectrum. However, these photodetectors generally exhibit slow response speed, thereby prolonging the generation of photocurrent matrices. Consequently, regardless of the type of spectrometer employed, these time-consuming processes for generating photocurrent matrix inherently delay real-time and fast spectral resolution, severely slowing down the data rate and hindering their applications in high-speed spectral communication. Therefore, it is urgent to reconfigure the miniaturized spectrometer architecture that seamlessly unifies high spectral resolution with high-speed data transmission, which will be a milestone for the next-generation SWC systems.

Over the past few decades, organic optoelectronic materials have emerged as transformative platforms for next-generation photonic devices, owing to their unparalleled advantages in tunable spectral absorption, solution processability, and intrinsic mechanical flexibility.[35–37] Extensive research on organic materials has created a rich organic material library, enabling precise and continuous absorption profile modulation from ultraviolet to near-infrared regions by merely tailoring molecular structures.[6,38–41] Consequently, these advances have significantly promoted the development of bulk-heterojunction (BHJ) organic photodetectors (OPDs) with customizable detection ranges, exceptional sensitivity, and ultrafast response speeds comparable to and even superior to the conventional inorganic counterparts in self-powered mode.[7,37,42–44] Furthermore, their inherent spectral programmability allows them to function dually as photoactive layers and wavelength-selective filters.[45] This unique synergy renders them ideal for miniaturized computational spectrometers that integrate OPDs with organic spectral filters, achieving tunable responsivities with considerable dissimilarities and nanosecond response times essential for advanced SWC.

Here, we proposed the SWC based on a high-performance, flexible, and miniaturized organic hyperspectrometer that concurrently integrates OPDs and organic spectral filters for the first time, establishing a new paradigm for SWC. In particular, we prepared 10 × 10 OPD arrays incorporating four distinct photoactive materials with varied photoresponse profiles. To further tune the responsivity of the OPD arrays, we introduced organic optical adjusting layers (OALs), which are composites of optoelectronic materials with different absorption profiles, on the backside of OPD arrays to work as spectral filters. Beyond the basic critical metrics of spectrometers, including broad spectral detection range (400–900 nm), high accuracy (0.60 nm), and high resolution (1.08 nm), the organic hyperspectrometer exhibits an impressive nanosecond response and gigabit-per-second data rates by fully utilizing the visible and near-infrared spectrum, ranking as the highest transmission rate among OWC based on organic optoelectronics. Moreover, the proposed organic hyperspectrometer successfully realized hardware-level encryption through dynamic spectral encoding. The proposed concept of integrating OPDs with organic filters can be extended to all-organic spectrometers, offering high spectral resolution, expansive bandwidth, and rapid response speeds. Benefitting from the high stability of corresponding flexible devices, high performance, and tunable sizes of the flexible organic hyperspectrometers, this work bridges the gap between high throughput and robust security by unifying spectral resolving and data transmission within a single flexible platform. This scalable framework not only surmounts OWC's bottlenecks but also pioneers ultracompact and intelligent optical systems, which is a critical leap toward the era of terahertz-scale data transmission and inherent security.

2. Working Process and Principle of the Spectral Communication System

Accordingly, the performance of computational spectrometers critically depends on the variability of their wavelength-dependent responsivities.[19] To maximize this dissimilarity, we first prepared OPD arrays using various organic photoactive materials with distinct absorption profiles, each exhibiting unique detection ranges. To further amplify this dissimilarity, we introduced optoelectronic organic materials on the backside of OPD arrays to function as the optical adjusting layer (OAL) with different absorption profiles, effectively modulating the response of each OPD. Consequently, the integration of variable responsivities of OPDs, paired with spectral-tunable organic filters, can efficiently modulate the response of OPD arrays and generate a highly dissimilar responsivity matrix. **Figure 1a** depicts the schematic of our organic hyperspectrometer, designed for high-speed encrypted SWC, which features OPD arrays with integrated OALs. Consequently, the organic hyperspectrometer can effectively reconstruct the unknown spectrum with high accuracy and high resolution.

To realize the SWC for high-speed encrypted information transmission, it is essential to precisely resolve the critical metrics of high-frequency modulated complex spectrum, including wavelength, modulation frequency, and binary state. Reconstructing the dynamic spectrum for SWC primarily contains four steps: 1) Calibrating the spectral responsivities of OPD arrays using a series of known monochromatic light to generate a responsivity matrix $(R((m,n),\lambda))$; 2) Programming high-frequency modulated optical signals (e.g., using light-emitting diodes (LEDs)I. Alimi, A. Shahpari, A. Sousa, R. Ferreira, P. Monteiro, and A. Teixeira. Challenges and opportunities of optical wireless communication technologies. In Pedro Pinho, editor, Optical Communication Technology, chapter 2. InTech, Rijeka, 2017a./laser diodes) to encode the high-speed binary-state information $(F(\lambda,t))$ in time domain, and then irradiating the organic

© 2025 Wiley-VCH GmbH

spectrometer; 3) Recording the photocurrent of OPD arrays irradiated by the programmed modulated incident light with binary states in the time domain and creating the photocurrent matrices $(I(m, n, t))$; 4) Reconstructing the modulated unknown spectrum $(F(\lambda, t))$ by combining and solving the responsivity $(R((m, n), \lambda))$ and photocurrent $(I((m, n), t))$ matrices using computational algorithms and decoding the encrypted optical signals for spectrum communication.[30]

Figures 1a–d illustrate the schematic concept and working principles of our hyperspectrometer for high-speed transmission of encrypted information. Essentially, composite optical signals, comprising multiple high-frequency modulated wavelengths encrypted with binary states (0 and 1), simultaneously irradiate the organic spectrometer, where "1" and "0" represent the "on" and "off" states of the light source (Figure 1a). As the resulting light is a composite spectrum generated by modulated spectrums with various binary states, OPD arrays commonly produce dynamic photoresponses whose waveform shapes diverge from those of individual input signals (Figure 1b). Consequently, it is impossible to accurately decrypt the input optical signals by analyzing the single-device waveform alone. To correctly decode the encrypted information, we need to resolve the spectrum at each binary state by synchronously combining the time-domain photoresponse across OPD arrays (e.g., at t_1, t_2, t_3, t_n, *etc.*). This spatial-temporal approach enables reconstruction of the original modulated spectrum.

By introducing the photocurrent of OPD arrays at each state in the computational algorithms and resolving the equation:

$$\int_{\lambda_i}^{\lambda_j} R((m, n), \lambda) \cdot F(\lambda, t) = I((m, n), t) \tag{1}$$

we can successfully reconstruct the dynamic spectrum at each state in the time domain, where $R((m, n), \lambda)$ is the responsivity of OPD subunit located at (m, n), $F(\lambda, t)$ is the function that represents the incident of light, and $I((m, n), t)$ is the photocurrent of OPD located at (m, n) at the specific time (t). Consequently, by resolving the wavelength, binary states, and modulation frequency of incident light, we can successfully decrypt the key metrics of encrypted input signals used for SWC (Figure 1d).

Based on the above analysis, we first fabricated high-speed organic hyperspectrometers via a solution-processing technique. As illustrated in **Figure 2a**, the miniaturized organic hyperspectrometer, featuring an OPD arrays with tunable responsivities and detection ranges, was fabricated through two primary steps: 1) Fabricating the OPD array with various organic material systems by sequentially spin-coating organic photoactive materials with various detection ranges; 2) Preparing the organic OAL arrays with different absorption profiles on the backside of OPD by combing spin-coating and photolithography technique (detailed in the Supplementary Note S2 and S3, Supporting Information). In principle, we can fabricate OPD arrays with any number or type of organic photoactive materials at will, offering significant design flexibility. To simplify the fabrication process while achieving a range of responsivities, we employed four distinct photoactive materials that were sequentially spin-coated onto ITO/Glass substrates following the procedure for individual OPD preparation. Subsequently, a photoresist layer was spin-coated on the glass side of the ITO/Glass substrate, which is patterned into grids matching the OPD unit dimensions. The organic OALs with tailored absorption profiles were then spin-coated within these grids to modulate the OPD responsivity without external packaging or integration. Such simple device architecture offers three significant advantages: 1) OPDs with same photoactive materials exhibit similar optoelectronic performance with minimal batch-to-batch and device-to-device variation, due to the easy solution-processing technique and simple device structure, facilitating the large-scale and low-cost industrial manufacture; 2) The modular design allows both photoactive materials and OAL materials to be readily substituted, providing more degrees of design for enhanced spectral resolution and broader applicability; 3) The entire OPD-OAL array can be prepared on a variety of rigid and flexible substrates, making it versatile for different application scenarios. As organic OALs reside on the backside of OPD arrays without involving any electronic dynamic activities, the resulting sub-unit OPDs can fully maintain their original optoelectronic performance, including low dark current, high specific detectivity, and fast response speed.[45] Here, we selected PM6:Y6, PBDB-T:FO-2Cl, PBDB-T:ITIC, and PBDB-T:F-M as the photoactive materials due to their distinct detection ranges and high response speeds in the pristine OPD. The detailed optoelectronic metrics of these materials are shown in Figures S1 and S2 (Supporting Information). As shown in Figure 2b, OPDs fabricated with four types of photoactive materials, individually examined, exhibit ultralow dark current of less than 10^{-9} A cm^{-2}, ensuring minimal noise current for the faint light detection. Moreover, the pristine OPDs (without OALs) exhibit high yet distinct responsivities across the visible to near-infrared region (spectrum range of 400–900 nm) at zero bias (Figure 2c). To further modulate the responsivity of OPDs, we introduced six types of organic optoelectronic materials as OALs. Notably, by finely tuning the weight ratios, concentrations of mixture solution, and the spin-coating parameters of OALs, the responsivity of OPDs can be flexibly and precisely adjusted (Figures S14, S17, and S19, Supporting Information). For high-accuracy and high-resolution spectrum reconstruction, OPD arrays must possess both high absolute responsivity and significant responsivity dissimilarity according to Equation 1 and a previous study.[31] If the responsivity curves of OPDs exhibit a linear relationship, it is impossible to reconstruct the spectrum via Equation 1. Therefore, incorporating a combination of narrowband and broadband devices with complementary spectral coverage will fast and efficiently determine the detection range. Benefitting from the tunable detection ranges of photoactive materials, it is feasible to prepare narrowband OPDs with tunable full-width at half maximum (FWHM). Collectively, these factors optimize the performance of the hyperspectrometer. As shown in Figure 2c and Figures S14, S17, and S19 (Supporting Information), the narrowband and broadband OPDs with OALs exhibit decreased but differentiated responsivities with considerable dissimilarities due to the varying absorption profiles of OALs. The detailed preparation process of OALs is provided in Supplementary Note S3 (Supporting Information).

Specific detectivity (D^*), a critical metric that qualifies the capability for detecting ultraweak optical signals, is defined as:

$$D^* = \frac{R\sqrt{AB}}{S_n} \tag{2}$$

© 2025 Wiley-VCH GmbH

15214095, 2026, 1, Downloaded from https://advanced.onlinelibrary.wiley.com/doi/10.1002/adma.202513003 by Yongsheng Chen - CAS-CHONGQING INSTITUTE OF GREEN & INTELLIGENT TECHNOLOGY , Wiley Online Library on [13/03/2026]. See the Terms and Conditions (https://onlinelibrary.wiley.com/terms-and-conditions) on Wiley Online Library for rules of use; OA articles are governed by the applicable Creative Commons License

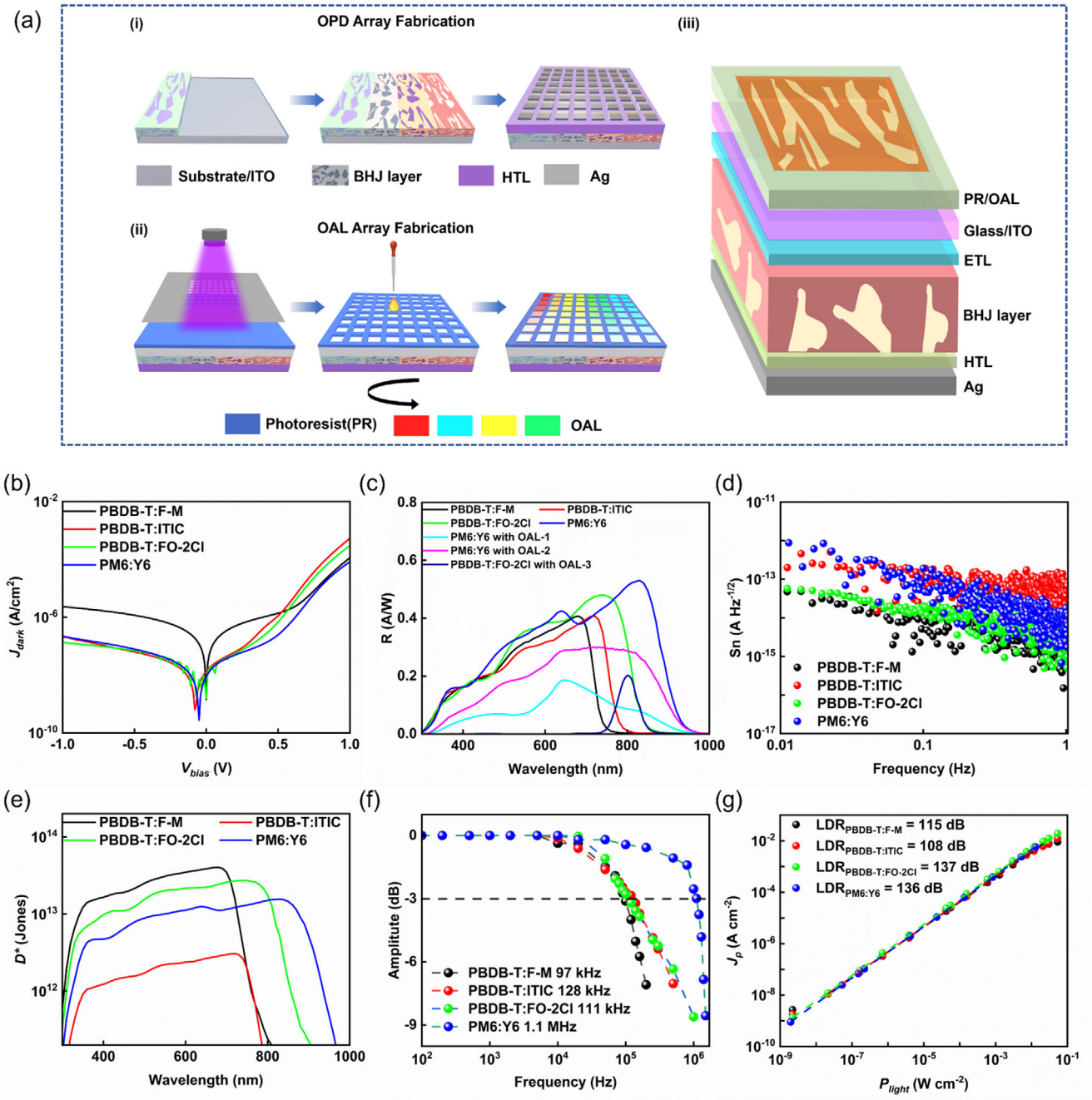

Figure 2. Optoelectronic performance of OPDs in an organic hyperspectrometer. a) The manufacturing process of an organic spectrometer and a Schematic of the OPD unit with OAL. We first prepared OPD arrays with four photoactive materials via a low-cost solution processing technique and fabricated OAL arrays by combining photolithography and solution processing technique. b) J-V curves of OPDs fabricated with four types of organic photoactive materials. c) Responsivity profiles of OPDs with OALs prepared using organic materials and bare OPDs without OALs. d) Noise spectral density in the dark of OPDs. e) D^* of OPDs. f) -3dB bandwidth of OPDs. g) LDR of OPDs.

where R, S_n, B, and A are responsivity, noise, bandwidth, and effective size of a photodetector, respectively.[6] The noise is obtained by conducting the Fast Fourier Transform of the dark current, which reaches less than 10^{-12} A Hz$^{-1/2}$ for all devices. Consequently, these four unmodulated devices exhibited a high D^* value over 10^{12} *Jones*, ensuring their capability to detect the ultraweak light signal in the SWC. While OAL-induced spectral filtering causes slight responsivity reductions and variations, OPDs with OALs exhibit correspondingly slight decreases and variations in D^* (Figure 2e; Figure S4, Supporting Information). Response speed, the most crucial parameter of OPD for high-speed OWC, is quantified by response time (t) and -3dB bandwidth (f_{-3dB}) (Figure 2f).[46] As shown in Figure S5 (Supporting Information), OPDs prepared with PM6:Y6, PBDB-T:FO-2Cl,

© 2025 Wiley-VCH GmbH

15214095, 2026, 1, Downloaded from https://advanced.onlinelibrary.wiley.com/doi/10.1002/adma.202513003 by Yongsheng Chen - CAS-CHONGQING INSTITUTE OF GREEN & INTELLIGENT TECHNOLOGY , Wiley Online Library on [13/03/2026]. See the Terms and Conditions (https://onlinelibrary.wiley.com/terms-and-conditions) on Wiley Online Library for rules of use; OA articles are governed by the applicable Creative Commons License

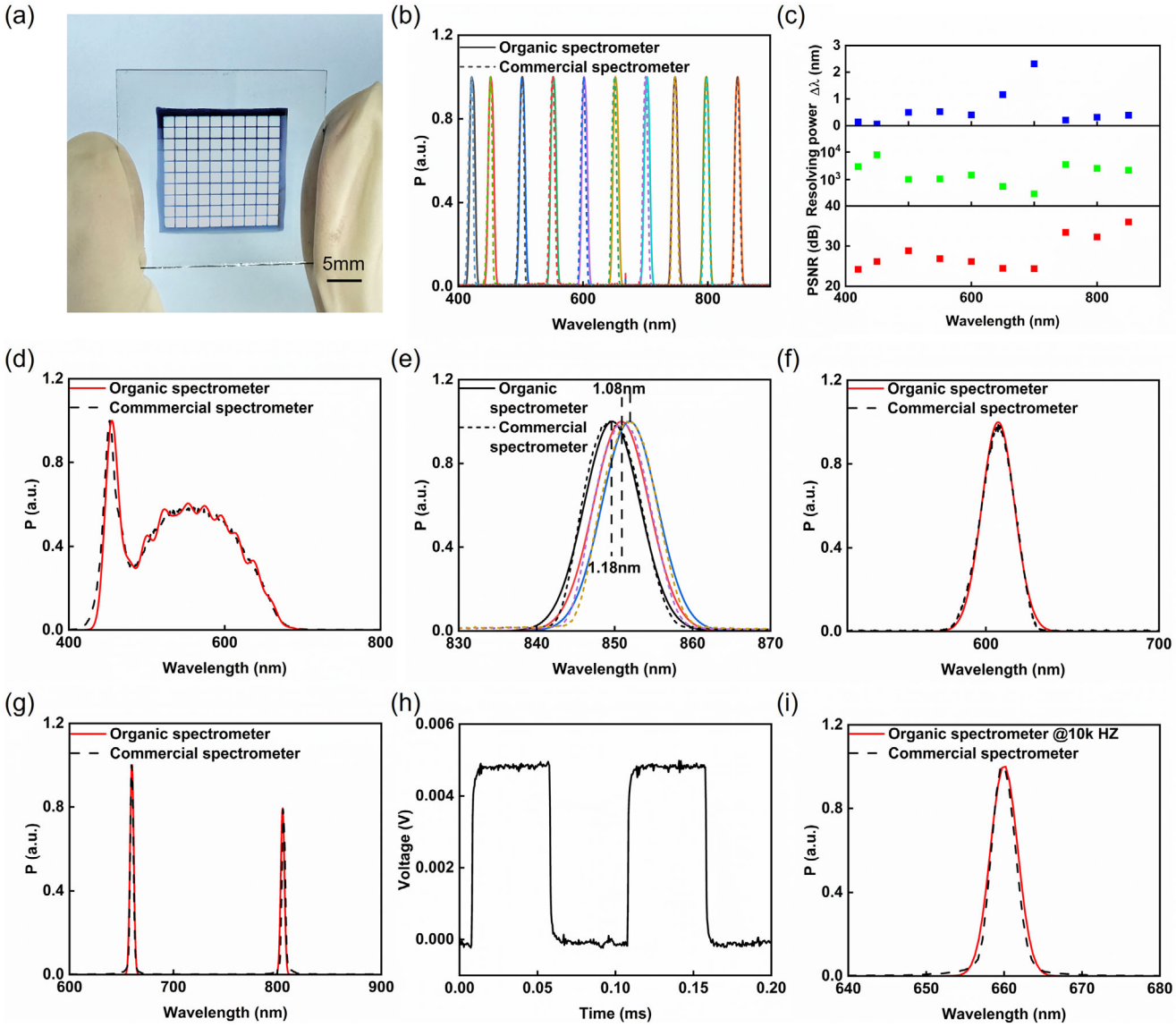

Figure 3. Demonstration of organic hyperspectrometers. a) Schematic of the optical image of an organic hyperspectrometer based on OPD arrays. b) Reconstructed quasi-monochromatic spectra (solid line) and their corresponding reference spectra measured by a commercial spectrometer (dashed line). c) The wavelength-resolving power (top), spectral accuracy: the peak wavelength difference between the reconstructed and reference spectra (middle), and the PSNR of our hyperspectrometer (bottom). d) Reconstructed spectra of broadband incident lights and its corresponding reference spectra. e) Reconstruction spectra of three types of light with similar wavelengths and their corresponding reference spectra. f) Reconstructed narrowband spectra and their corresponding reference spectra. g) visible and NIR light reconstructed via the organic hyperspectrometer at the same time. h, i) The reconstruction of a high-frequency (10 KHz) dynamic narrowband spectrum.

PBDB-T:ITIC, and PBDB-T:F-M, exhibit a short response time of 684 ns, 7.54, 5.13, and 7.06 µs, respectively, with corresponding f_{-3dB} of 1.1 MHz, 111 kHz, 128 kHz, and 97 kHz. In our organic hyperspectrometer, OALs deposited on the backside of OPD did not involve any electronic dynamic activities in OPDs; therefore, the OAL-modulated OPDs fully preserve the high-speed response of pristine OPDs, ensuring high-speed data transmission in the SWC.[45] Linear dynamic range (LDR) is defined as:

$$\mathrm{LDR} = 20 \log \frac{J_{upper}}{J_{lower}} \tag{3}$$

where J_{upper} and J_{lower} (A cm^{-2}) stand for the maximum and minimum output photocurrent values, respectively.[42] As shown in Figure 2g, all these devices exhibit an LDR value of over 100 dB, ensuring stable and reproducible operation over a broad illumination range, which is a prerequisite for a spectral communication system to adapt to complex environments.

Figure 3a depicts the optical image of the rigid organic hyperspectrometer fabricated with OPD arrays, which exhibits a pixel pitch of 1500 µm, a fill factor of 65%, and a total active area of 1.7 × 1.7 cm^2. As the size of the OPD is primarily determined by the area size of top electrodes prepared by the thermal

© 2025 Wiley-VCH GmbH

15214095, 2026, 1, Downloaded from https://advanced.onlinelibrary.wiley.com/doi/10.1002/adma.202513003 by Yongsheng Chen - CAS-CHONGQING INSTITUTE OF GREEN & INTELLIGENT TECHNOLOGY , Wiley Online Library on [19/03/2026]. See the Terms and Conditions (https://onlinelibrary.wiley.com/terms-and-conditions) on Wiley Online Library for rules of use; OA articles are governed by the applicable Creative Commons License

deposition approach via a predesigned shadow mask, it is feasible to tune the spectrometer dimension by simply adjusting the size and the shape of the shadow mask. To further miniaturize the size of the organic spectrometer, we prepared OPD with a pixel pitch of 300 μm, and the total size of the organic spectrometer is 4 × 4 mm^2 (Figure S9 and Supplementary Note S2, Supporting Information). The small-sized organic hyperspectrometer successfully reconstructed the narrowband and quasi-monochromatic light (Figure S10, Supporting Information). As the organic hyperspectrometer was prepared with independent OPD units, it can effectively eliminate the electrical crosstalk effect during the photocurrent measurement, ensuring a reliable and reproducible spectrum reconstruction in real-world applications. Moreover, by simultaneously collecting the photocurrent of these OPD arrays, it is feasible to rapidly reconstruct the spectrum and boost the communication speed.

To validate the high performance of our organic hyperspectrometer, we first reconstructed the quasi-monochromatic light (FWHM ≈8 nm) across a wide spectral range from 400 to 900 nm, which agrees well with the reference spectrum recorded by a commercial spectrometer (Figure 3b, dashed line) across this full spectral range. Here, we introduced the spectrum accuracy $\Delta\lambda$ ($\Delta\lambda$: the peak difference between the reconstructed spectrum and the reference spectrum), resolving power ($R_\lambda = \lambda/\Delta\lambda$), and peak signal-to-noise ratio (PSNR) to quantitatively assess the fidelity of spectrum reconstruction.[30] As shown in Figure 3c, our organic hyperspectrometer exhibits an average accuracy $\Delta\lambda$ of 0.60 nm, a wavelength resolving power of up to 2000, and a PSNR of 28 dB, demonstrating excellent consistency with the reference spectra measured using a commercial spectrometer.

Spectral resolution, defined as the capability to distinguish between the closest pair of spectral peaks, plays a crucial role in determining the spectrum utilization efficiency in the SWC system. Therefore, high spectral resolution will significantly contribute to the data transmission speed and capacity in the SWC system. To assess this, we illuminated the organic hyperspectrometer with densely spaced monochromatic light from ≈840 to 860 nm and successfully resolved features with a spectral resolution as fine as 1.08 nm (Figure 3d). Taking advantage of OPDs' high response in the whole spectral range of 400–900 nm, the organic hyperspectrometer also accurately reconstructs various quasi-monochromatic (FWHM = 4 nm) and narrowband spectra (FWHM = 30 nm) across the entire spectrum range. Beyond the monochromatic light reconstruction, we have also verified the capability of our organic hyperspectrometer to reconstruct narrow and broad spectra. As depicted in Figures 3e,f, the reconstructed narrow spectra via the organic hyperspectrometer are all highly consistent in both shape and central peak positions with the reference spectra obtained from the commercial spectrometer (Figures 3e,f). When irradiating the device using the broadband white light ranging from 400 to 700 nm, the organic hyperspectrometer successfully reconstructs the spectrum with high fidelity, confirming its robustness and applicability for broadband SWC.

The high-performance spectral analysis of the organic hyperspectrometer, combined with its fast response speed, facilitates dynamic spectrum reconstruction within a nanosecond timescale. To verify this capability, we illuminated the device with a narrowband light modulated at 10 kHz (Figure 2h) for dynamic spectrum reconstruction. As shown in Figure 2h, the reconstructed spectra reliably reproduce the time-varying spectral shape measured by a commercial instrument, indicating that the high-speed organic hyperspectrometer can effectively capture the dynamic spectrum for the high-speed SWC.

3. High-Speed Encrypted Spectral Wireless Communication

The advances in fast dynamic spectrum reconstruction naturally lead to applications in spectral communication, improving communication speed and security. **Figure** 4a presents the schematic of the high-speed SWC and encryption process, highlighting its dual advantages in boosting data transmission speed and security. Briefly, at the transmission stage, the digital message to be transmitted is translated into binary bitstreams (e.g., 0 101 1100...) via a wave generator, which drives lasers to generate corresponding binary optical signals (e.g., 0 101 1100...). The "1" and "0" represent "on" and "off" states of targeted lights, respectively. To generate an encrypted composite spectrum, multiple lasers dynamically driven by separate waveform generators were combined to produce intricate spectral signatures. For accurate and high-speed decryption in optical communication, it is essential to precisely reconstruct the complete dynamic spectral profile, including wavelength, modulation frequency, and on/off binary states. This level of spectral decoding can only be achieved via advanced spectroscopic reconstruction techniques.

By recording the photocurrent of each OPD subunit under the encrypted spectrum irradiation, we can create a data set of photocurrents for spectral reconstruction. By integrating the photocurrent data set, responsivity matrix, and algorithms, it is feasible to reconstruct the dynamic spectrum in the time domain. To demonstrate the spectral communication and information encryption process, we utilized three high-frequency modulated optical communication wavelengths (660, 530, and 440 nm) as communication channels, serving as encryption keys to encode the letters "N", "K", and "U", respectively. Notably, the individual OPD exhibited indiscriminate responses to composite light inputs (Figure 4b; Figure S15, Supporting Information), rendering it impossible to decipher the input optical information. However, when reconstructing the high-frequency dynamic spectrum using the organic hyperspectrometer via the multiplexing principle, we successfully resolved temporal wavelength variations in the time domain (Figure 4c). By translating the data of wavelength profiles dependent on time, we can correctly decrypt the encrypted information carried by three optical signals, further demonstrating the advantages of this encryption approach in enhancing information security (Figure 4d). To quantify the transmission rate of the spectrometer, we first evaluated the bit error rate (BER) using a non-return-to-zero (NRZ) modulation scheme. Generally, the BER should be $<3.8 \times 10^{-3}$ to achieve reliable optical communication, which is under 7% pre-forward-error-correction (pre-FEC). As shown in Figure 4e, the OPD with the response time of 684 ns demonstrates a maximum achievable data rate of 20 Mbps with a BER of 3.7×10^{-3}. To visualize the BER of the OPD at different transmission rates, we also conducted an eye-diagram analysis with an intrinsic rate of 20 Mbps, which showed an open and clear eye diagram, further indicating that the OPD can be readily used for practical optical communication. In

© 2025 Wiley-VCH GmbH

15214095, 2026, 1, Downloaded from https://advanced.onlinelibrary.wiley.com/doi/10.1002/adma.202513003 by Yongsheng Chen - CAS-CHONGQING INSTITUTE OF GREEN & INTELLIGENT TECHNOLOGY , Wiley Online Library on [13/03/2026]. See the Terms and Conditions (https://onlinelibrary.wiley.com/terms-and-conditions) on Wiley Online Library for rules of use; OA articles are governed by the applicable Creative Commons License

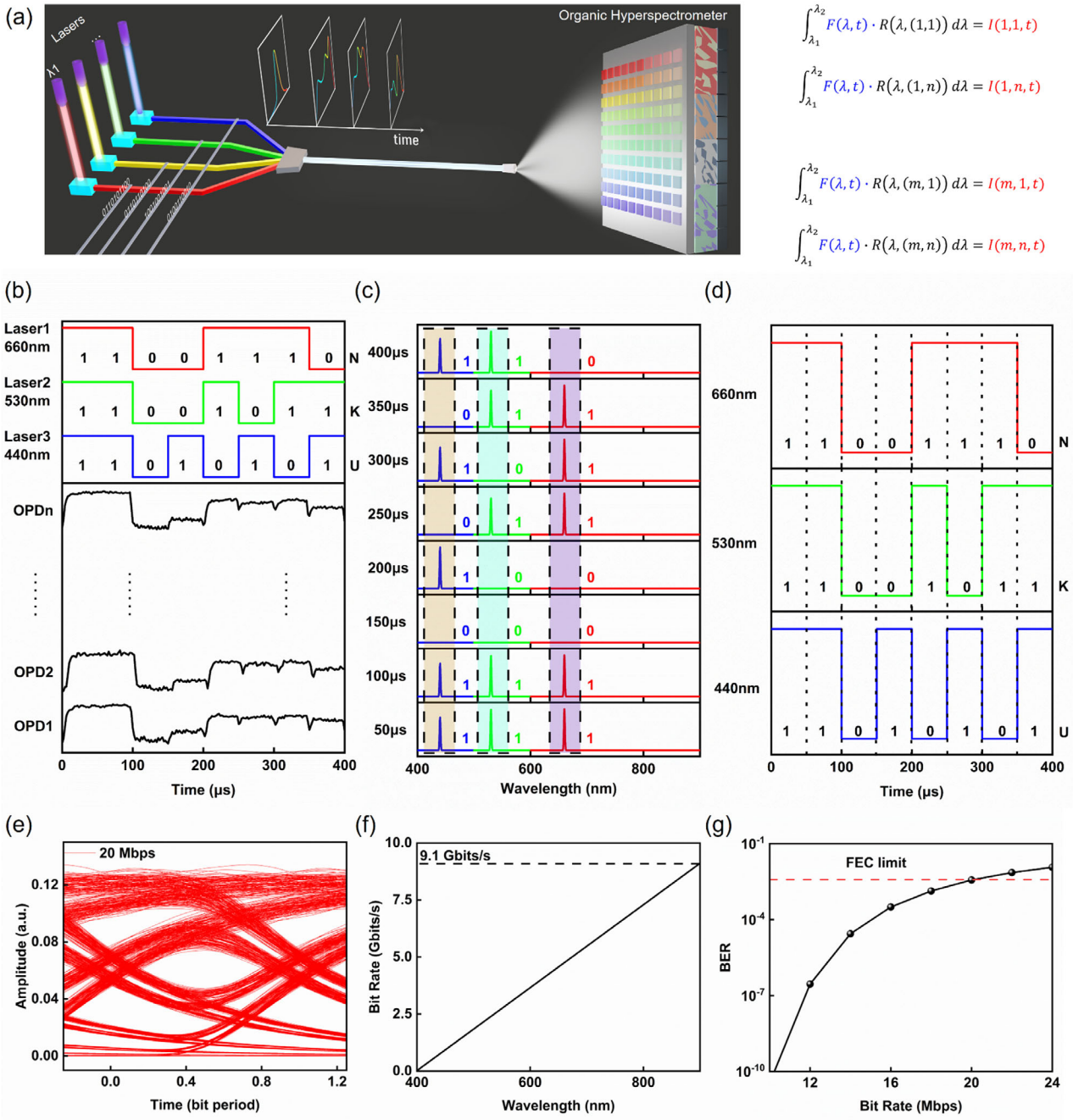

Figure 4. High-speed encrypted spectral wireless communication based on organic hyperspectrometers. a) Schematic diagram of encrypted SWC. b) The input signals of high-frequency modulated lasers with different wavelengths and the corresponding photocurrent of OPDs in organic hyperspectrometers. c) The reconstructed spectrum in the time domain. d) Extraction of the encrypted optical information via the organic hyperspectrometer for SWC. e) Eye diagram of a single OPD with a response time of 684 ns at a communication rate of 20 Mbps. f) Theoretical data transmission rate dependent on the spectral range from 400 to 900 nm. g) The BER of the OPD with a response time of 684 ns.

the SWC system, the overall theoretical data rate is determined by the single OPD data rate, detection range, and hyperspectrometer spectral resolution, which can be calculated as:

$$\text{System Rate} = Data\ Rate_{Single\ OPD} \times \frac{Detection\ Range}{Spectral\ Resolution} \quad (4)$$

Therefore, improving the system rate, it is essential to increase these three critical parameters. Benefiting from the high resolution (≈1 nm) and broad bandwidth (400–900 nm) of our organic spectrometer, the theoretical transmission speed of our spectrometer can reach 9.1 Gbits/s by slicing the broad spectrum into ≈500 channels (Figure 4f), ranking as the highest speed among OWC systems based on organic materials (Table S1,

© 2025 Wiley-VCH GmbH

15214095, 2026, 1, Downloaded from https://advanced.onlinelibrary.wiley.com/doi/10.1002/adma.202513003 by Yongsheng Chen - CAS-CHONGQING INSTITUTE OF GREEN & INTELLIGENT TECHNOLOGY , Wiley Online Library on [19/03/2026]. See the Terms and Conditions (https://onlinelibrary.wiley.com/terms-and-conditions) on Wiley Online Library for rules of use; OA articles are governed by the applicable Creative Commons License

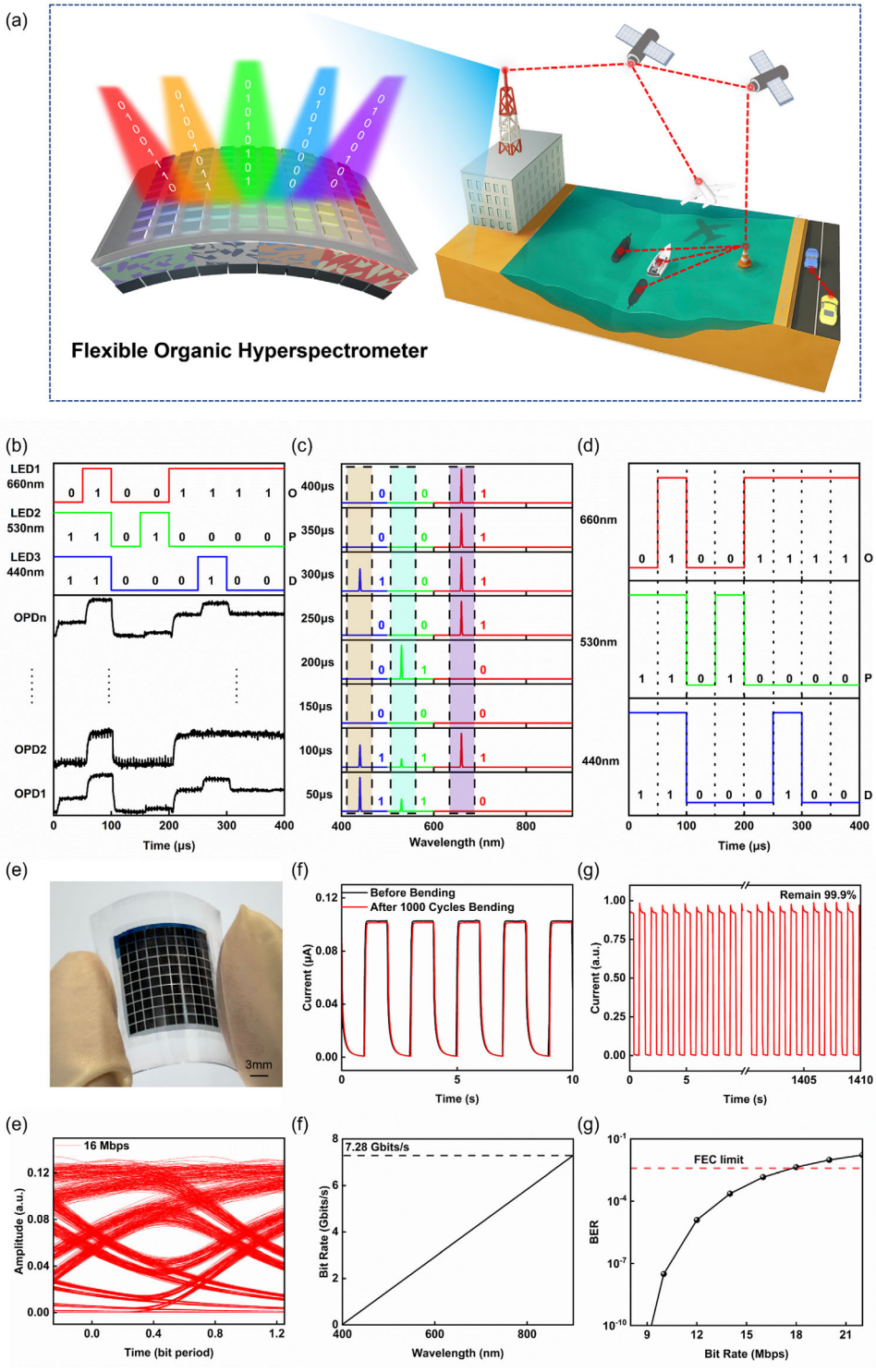

Figure 5. High-speed encrypted spectral wireless communication based on the flexible organic hyperspectrometer. a) Application scenarios of encrypted SWC based on the flexible organic spectrometers: satellites and drone communications, submarine operations, and intelligent cars. b) The input signals of high-frequency modulated lasers with different wavelengths and the corresponding photocurrent of OPDs in flexible organic hyperspectrometers. c) The reconstructed high-frequency modulated spectrum in the time domain. d) Extraction of the encrypted optical information via the flexible organic hyperspectrometer for encrypted SWC. e) Optical image of flexible organic hyperspectrometer in bending state. f) I–T curves of the flexible organic hyperspectrometers before and after bending 1000 cycles under 650 nm light illumination at zero bias. g) Cyclic stability of flexible organic hyperspectrometer under ambient light. h) Eye diagram of flexible organic hyperspectrometer at a communication rate of 16 Mbps. i) The data transmission rate of the flexible organic hyperspectrometer is dependent on the spectrum range from 400 to 900 nm. j) The BER of the flexible organic hyperspectrometer in different transmission rates.

© 2025 Wiley-VCH GmbH

15214095, 2026, 1, Downloaded from https://advanced.onlinelibrary.wiley.com/doi/10.1002/adma.202513003 by Yongsheng Chen - CAS-CHONGQING INSTITUTE OF GREEN & INTELLIGENT TECHNOLOGY , Wiley Online Library on [13/03/2026]. See the Terms and Conditions (https://onlinelibrary.wiley.com/terms-and-conditions) on Wiley Online Library for rules of use; OA articles are governed by the applicable Creative Commons License

Supporting Information). Unlike conventional optical MIMO systems, which utilize a handful of discrete channels for point-to-point links, our platform can reconstruct any high-frequency modulated spectrum within the detection range for SWC, enabling the simultaneous use of monochromatic, narrowband, and broadband light. This versatility not only exponentially increases transmission rates but also introduces multi-layered security, which is a transformative leap toward high-speed, secure optical communication.

4. Flexible Device for Encrypted Wireless Spectral Communication

Flexible SWC system marks a transformative leap in spectroscopic technology, enabling bendable configurations that seamlessly integrate with curved substrates while delivering unprecedented adaptability, portability, and multifunctionality. **Figure** 5a illustrates the versatile deployment potential of these flexible and lightweight spectrometers across various scenarios, including the SWC between satellites and drones, submarine operations, and intelligent cars that require high-speed and security data communication. Leveraging the inherent solution-processable nature of OPDs and the intrinsic flexibility of organic materials, we fabricated a high-performance flexible spectrometer on a PET-ITO substrate, employing fabrication protocols analogous to those used for rigid devices. The detailed fabrication process is described in Supplementary Note S2 (Supporting Information).

As shown in Figure S13 (Supporting Information), the flexible organic hyperspectrometer exhibited a comparable performance to that of a rigid device regarding average spectral accuracy (0.49 nm), wavelength resolving power (2200) and PSNR (28.86 dB) (Figure S13, Supporting Information) when reconstructing the spectrum following same reconstruction workflow outlined in Supplementary note S6 (Supporting Information). Furthermore, the device demonstrated exceptional fidelity in reconstructing quasi-monochromatic and narrowband spectra, which is a prerequisite for reliable spectral communication (Figure S13, Supporting Information). Similar to their rigid counterparts, the high-speed flexible organic hyperspectrometer demonstrated identical capabilities for accurately measuring the dynamic spectrum. As illustrated in Figure 5b, when exposed to high-frequency modulated composite light, the OPD subunits generated distinct responses that were aligned with the preset input signals. By applying multiplexing principles, the system successfully decoded both spectral profiles and embedded data. As shown in Figures 5b–d, the flexible organic hyperspectrometer successfully decrypted the information of "O", "P", and "D" carried by three wavelengths of 660, 530, and 440 nm, respectively, which is well aligned with the preset encrypted information.

Figure 5e shows the optical image of the resulting flexible spectrometer in bending states. Stability remains a paramount factor for flexible devices in real-world applications. Remarkably, the flexible OPD subunits of the organic spectrometer retained more than 99.9% of their initial photoresponse after operating 1400 on-off switching cycles and maintained more than 99.0% of their original performance following 1000 bending cycles, highlighting their robustness (Figure 5f). Even after 1000 bending cycles, the device exhibited negligible photocurrent drift, confirming its durability under stress (Supplementary Note S5, Supporting Information). To evaluate scenario-specific adaptability, we tested the spectral reconstruction quality of the device under the bending state. As shown in Figure S21 (Supporting Information), the flexible organic hyperspectrometer successfully realizes dynamic spectrum reconstruction and encrypted spectral communication, demonstrating its significant potential for high-speed encrypted spectral communication in future flexible electronics. Through non-return-to-zero (NRZ) modulation, the slowest-response OPD achieved a maximum data rate of 16 Mbps with clear eye diagrams (Figure 5h), while full-spectrum utilization (400–900 nm) enabled a theoretical transmission rate of 7.28 Gbits s^{-1}, ranking as the highest optical communication speed among flexible organic optical communication systems (Table S1, Supporting Information). As established earlier, the data transmission rate of the organic hyperspectrometer depends on three key factors: spectral resolution, detection range, and the intrinsic data rate of each OPD. While rigid and flexible devices exhibit comparable spectral resolution and detection range, rigid OPDs achieve higher intrinsic data rates due to their inherent faster photoresponse, leading to a high data transmission rate in the system. As shown in Figures S23a–c (Supporting Information), the flexible device exhibits higher series resistance and capacitance (resulting in a larger τ_{RC}) and lower charge mobility. Taken together, these factors lead to a slower response speed in the flexible device (Figures S23a–c, Supporting Information). All characteristics are closely linked to the quality of the ITO substrate. Figures S23d–e (Supporting Information) reveal that the flexible PET/ITO substrate has higher surface roughness and lower transparency than the rigid substrate, attributable to differences in ITO electrode growth parameters across substrates. The quality of the ITO electrode directly affects OPD performance, including response speed, responsivity, and noise. The combination of mechanical endurance, precision, and superior high-speed performance positions the flexible organic hyperspectrometer as a groundbreaking platform for next-generation spectral communication technologies.

5. Conclusion

In this work, we presented a high-speed SWC platform enabled by a flexible, miniaturized organic hyperspectrometer that integrates OPD arrays with tunable organic spectral filters. The SWC achieved a broad spectral detection range (400–900 nm), ultrafast nanosecond-level response times, and a theoretical data rate of 9.1 Gbits s^{-1}, ranking as the highest reported for organic optoelectronic-based OWC. By decoding the rich information carried by the dynamic, complex spectrum through resolving the wavelength, modulation frequency, and binary state, we successfully realized an ultrafast transmission rate and hardware-level encryption, which effectively addressed the bottlenecks of inefficient spectral utilization and the inherent vulnerabilities of optical communication. Moreover, the intrinsic flexibility and bandgap tunability of organic materials enable scalable, portable, and adaptive deployment, further expanding their applications in emerging scenarios. While the organic SWC system achieves unprecedented data rates, scaling to terahertz-level transmission will require extending the operational bandwidth into the infrared and UV regions. Additionally, optimizing OPD subunit response speeds to tens of nanoseconds could further elevate data

© 2025 Wiley-VCH GmbH

15214095, 2026, 1, Downloaded from https://advanced.onlinelibrary.wiley.com/doi/10.1002/adma.202513003 by Yongsheng Chen - CAS-CHONGQING INSTITUTE OF GREEN & INTELLIGENT TECHNOLOGY , Wiley Online Library on [19/03/2026]. See the Terms and Conditions (https://onlinelibrary.wiley.com/terms-and-conditions) on Wiley Online Library for rules of use; OA articles are governed by the applicable Creative Commons License

rates, while incorporating light phase modulation could unlock new dimensions for high transmission rate and encryption. Future work should focus on developing novel organic material systems with enhanced charge mobility and broader spectral coverage. Overview: this SWC platform bridges the gap between ultrahigh-speed data transmission and robust security, offering a scalable framework for next-generation optical networks. By harmonizing the tunability of organic materials with ultrafast spectral analysis, our work paves the way for ultracompact, intelligent communication systems that can meet the demands of a hyperconnected and data-driven world.

Acknowledegments

The authors gratefully acknowledge financial support from the National Key R&D Program of China (2022YFB4200400) and the Natural Science Foundation of Tianjin, China (23JCZDJC01160).

Supporting Information

Supporting Information is available from the Wiley Online Library or from the author.

Conflict of Interest

The authors declare no conflict of interest.

Data Availability Statement

The data that support the findings of this study are available from the corresponding author upon reasonable request.

Keywords

flexible organic spectrometers, hyperspectrometers, organic photodetectors, spectral wireless communication

Received: July 8, 2025
Revised: August 18, 2025
Published online: September 8, 2025

[1] A. Rizzo, A. Novick, V. Gopal, B. Y. Kim, X. Ji, S. Daudlin, Y. Okawachi, Q. Cheng, M. Lipson, A. L. Gaeta, K. Bergman, *Nat. Photonics* **2023**, *17*, 781.
[2] R. J. Essiambre, R. W. Tkach, *Proceedings of the IEEE* **2012**, *100*, 1035.
[3] P. Yang, Y. Xiao, M. Xiao, S. Li, *IEEE Network* **2019**, *33*, 70.
[4] S. Soderi, A. Brighente, S. Xu, M. Conti, *IEEE Trans. Mob. Comput.* **2024**, *23*, 15182.
[5] P. J. Winzer, D. T. Neilson, A. R. Chraplyvy, *Opt. Express* **2018**, *26*, 24190.
[6] Y. Xia, J. Zhang, T. Guo, H. Wang, C. Geng, Y. Zhu, R. Han, Y. Yang, G. Song, X. Wan, G. Li, Y. Chen, *Adv. Funct. Mater.* **2025**, *35*, 2412813
[7] Y. Zhu, H. Chen, R. Han, H. Qin, Z. Yao, H. Liu, Y. Ma, X. Wan, G. Li, Y. Chen, *Natl. Sci. Rev.* **2023**, *11*, nwad311.
[8] X. Zhang, G. Klevering, X. Lei, et al., *ACM Comput. Surv.* **2023**, *55*, 329.
[9] I. Alimi, A. Shahpari, A. Sousa, R. Ferreira, P. Monteiro, A. Teixeira, *Optical Communication Technology*, InTech, Rijeka, chapter 2, **2017**, 5–44.
[10] N. Su, E. Panayirci, M. Koca, A. Yesilkaya, H. V. Poor, H. Haas, *IEEE Trans. Commun.* **2021**, *69*, 2585.
[11] Z. Wang, Y. Gao, Y. Li, H. Yan, F. Kang, Y. Shen, X. P. Zhang, G. Wei, H. Fu, *Adv. Funct. Mater.* **2024**, *34*, 2310911
[12] D. Lowndes, S. Frick, A. Hart, J. Rarity, *EPJ Quantum Technol.* **2021**, *8*, 15.
[13] M. Lanza, A. Sebastian, W. D. Lu, M. Le Gallo, M.-F. Chang, D. Akinwande, F. M. Puglisi, H. N. Alshareef, M. Liu, J. B. Roldan, *Science* **2022**, *376*, abj9979.
[14] A. Dodda, S. Subbulakshmi Radhakrishnan, T. F. Schranghamer, D. Buzzell, P. Sengupta, S. Das, *Nat. Electron.* **2021**, *4*, 364.
[15] H. O. Çirkinoğlu, O. Ferhanoğlu, G. Karabulut Kurt, *Opt. Commun.* **2021**, *485*, 126752.
[16] P. A. Haigh, A. Burton, K. Werfli, H. L. Minh, E. Bentley, P. Chvojka, W. O. Popoola, I. Papakonstantinou, S. Zvanovec, *IEEE J. Sel. Areas Commun.* **2015**, *33*, 1771.
[17] G. Figueiredo, R. A. S. Ferreira, P. S. André, *J. Opt. Commun. Netw.* **2024**, *16*, D1.
[18] C. E. Mejia, C. N. Georghiades, *IEEE Trans. Commun.* **2019**, *67*, 4955.
[19] Z. Yang, T. Albrow-Owen, W. Cai, T. Hasan, *Science* **2021**, *371*, abe0722
[20] Q. Xue, Y. Yang, W. Ma, H. Zhang, D. Zhang, X. Lan, L. Gao, J. Zhang, J. Tang, *Adv. Sci.* **2024**, *11*, 2404448
[21] A. Ravindran, D. Nirmal, P. Prajoon, D. G. N. Rani, *IEEE Sens. J.* **2021**, *21*, 5645.
[22] H. Li, X. Peng, C. Guan, H. Hu, *Micromachines* **2022**, *13*, 1689
[23] T. A. Kwa, R. F. Wolffenbuttel, *Sens. Actuators A: Phys.* **1992**, *31*, 259.
[24] H. H. Yoon, H. A. Fernandez, F. Nigmatulin, W. Cai, Z. Yang, H. Cui, F. Ahmed, X. Cui, Md. G. Uddin, E. D. Minot, H. Lipsanen, K. Kim, P. Hakonen, T. Hasan, Z. Sun, *Science* **2022**, *378*, 296.
[25] W. Deng, Z. Zheng, J. Li, R. Zhou, X. Chen, D. Zhang, Y. Lu, C. Wang, C. You, S. Li, L. Sun, Y. Wu, X. Li, B. An, Z. Liu, Q. J. Wang, X. Duan, Y. Zhang, *Nat. Commun.* **2022**, *13*, 4627.
[26] G. Cai, Y. Li, Y. Zhang, X. Jiang, Y. Chen, G. Qu, X. Zhang, S. Xiao, J. Han, S. Yu, Y. Kivshar, Q. Song, *Nat. Mater.* **2024**, *23*, 71.
[27] X. He, Y. Li, H. Yu, G. Zhou, L. Ke, H.-L. Yip, N. Zhao, *Nat. Electron.* **2024**, *7*, 694.
[28] L. Guo, H. Sun, M. Wang, M. Wang, L. Min, F. Cao, W. Tian, L. Li, *Adv. Mater.* **2022**, *34*, 2200221
[29] H. Kim, S. Z. Uddin, D. H. Lien, M. Yeh, N. S. Azar, S. Balendhran, T. Kim, N. Gupta, Y. Rho, C. P. Grigoropoulos, K. B. Crozier, A. Javey, *Nature* **2021**, *596*, 232.
[30] Y. Zhu, Z. Zhang, H. Qin, Y. Yang, J. Zhang, Z. Yao, G. Li, Y. Chen, *Adv. Mater.* **2025**, *37*, 2502608.
[31] Z. Yang, T. Albrow-Owen, H. Cui, J. Alexander-Webber, F. Gu, X. Wang, T. C. Wu, M. Zhuge, C. Williams, P. Wang, A. V. Zayats, W. Cai, L. Dai, S. Hofmann, M. Overend, L. Tong, Q. Yang, Z. Sun, T. Hasan, *Science* **2019**, *365*, 1017.
[32] J. Bao, M. G. Bawendi, *Nature* **2015**, *523*, 67.
[33] C. Huang, Y. Chen, X. L. Wang, et al., *ACS Appl. Mater. Interfaces* **2023**, *15*, 7129
[34] X. Zhu, L. Bian, H. Fu, et al., *Light Sci. Appl.* **2020**, *9*, 73.
[35] J. Yi, G. Zhang, H. Yu, H. Yan, *Nat. Rev. Mater.* **2024**, *9*, 46.
[36] K. Zhang, J. Wu, C. Sun, D. S. Chung, Y. Geng, L. Ye, *Nat. Rev. Mater.* **2025**, *10*, 487.
[37] P. C. Y. Chow, T. Someya, *Adv. Mater.* **2020**, *32*, 1902045.
[38] J. Liu, M. Gao, J. Kim, Z. Zhou, D. S. Chung, H. Yin, L. Ye, *Mater. Today* **2021**, *51*, 475.
[39] H. Yao, J. Wang, Y. Xu, S. Zhang, J. Hou, *Acc. Chem. Res.* **2020**, *53*, 822.
[40] X. Wan, C. Li, M. Zhang, Y. Chen, *Chem. Soc. Rev.* **2020**, *49*, 2828.
[41] Y. Xia, C. Geng, X. Bi, et al., *Adv. Opt. Mater.* **2024**, *12*, 2301518.

© 2025 Wiley-VCH GmbH

15214095, 2026, 1, Downloaded from https://advanced.onlinelibrary.wiley.com/doi/10.1002/adma.202513003 by Yongsheng Chen - CAS-CHONGQING INSTITUTE OF GREEN & INTELLIGENT TECHNOLOGY , Wiley Online Library on [13/03/2026]. See the Terms and Conditions (https://onlinelibrary.wiley.com/terms-and-conditions) on Wiley Online Library for rules of use; OA articles are governed by the applicable Creative Commons License

[42] D. Yang, D. Ma, *Adv. Opt. Mater.* **2019**, *7*, 1800522.
[43] H. Ren, J.-D Chen, Y. Q. Li, J. X. Tang, *Adv. Sci.* **2021**, *8*, 2002418.
[44] Y. Zhu, J. Zhang, H. Qin, G. Song, Z. Yao, Z. Quan, Y. Yang, X. Wan, G. Li, Y. Chen, *Appl. Phys. Lett.* **2024**, *124*, 061104.
[45] Y. Zhu, H. Qin, T. Guo, Y. Yang, Z. Zhang, J. Zhang, M. Li, H. Chen, S. Wu, R. Han, X. Wan, G. Li, Y. Chen, *Sci. China Mater.* **2024**, *67*, 852.
[46] W. Shi, Q. Han, Y. Zhu, Y. Xia, T. He, S. Wang, L. Li, W. Ma, G. Long, G. Li, Z. Yao, C. Li, X. Wan, Y. Chen, *Natl. Sci. Rev.* **2024**, *12*, nwae409.

© 2025 Wiley-VCH GmbH

15214095, 2026, 1, Downloaded from https://advanced.onlinelibrary.wiley.com/doi/10.1002/adma.202513003 by Yongsheng Chen - CAS-CHONGQING INSTITUTE OF GREEN & INTELLIGENT TECHNOLOGY , Wiley Online Library on [19/03/2026]. See the Terms and Conditions (https://onlinelibrary.wiley.com/terms-and-conditions) on Wiley Online Library for rules of use; OA articles are governed by the applicable Creative Commons License